Pressure-Induced Metallization of Molybdenum Disulfide

Zhen-Hua Chi,[1] Xiao-Miao Zhao,[2,3] Haidong Zhang,[4] Alexander F. Goncharov,[1,4] Sergey S. Lobanov,[4,5]
Tomoko Kagayama,[6,*] Masafumi Sakata,[6] and Xiao-Jia Chen[1,2,4,†]

[1]*Key Laboratory of Materials Physics, Institute of Solid State Physics, Chinese Academy of Sciences,
Hefei 230031, People's Republic of China*
[2]*Center for High Pressure Science and Technology Advanced Research, Shanghai 201203, People's Republic of China*
[3]*Department of Physics, South China University of Technology, Guangzhou 510640, People's Republic of China*
[4]*Geophysical Laboratory, Carnegie Institution of Washington, Washington, D.C. 20015, USA*
[5]*V.S. Sobolev Institute of Geology and Mineralogy SB RAS, Novosibirsk 630090, Russia*
[6]*KYOKUGEN, Center for Quantum Science and Technology under Extreme Conditions, Osaka University, Osaka 560-8531, Japan*
(Received 10 December 2013; revised manuscript received 2 June 2014; published 16 July 2014)

X-ray diffraction, Raman spectroscopy, and electrical conductivity measurements of molybdenum disulfide MoS_2 are performed at pressures up to 81 GPa in diamond anvil cells. Above 20 GPa, we find discontinuous changes in Raman spectra and x-ray diffraction patterns which provide evidence for isostructural phase transition from $2H_c$ to $2H_a$ modification through layer sliding previously predicted theoretically. This first-order transition, which is completed around 40 GPa, is characterized by a collapse in the c-lattice parameter and volume and also by changes in interlayer bonding. After the phase transition completion, MoS_2 becomes metallic. The reversibility of the phase transition is identified from all these techniques.

Molybdenum disulfide (MoS_2), which has a finite band-gap in monolayer manifestation, is currently under intensive examination as the alternative and/or complement to graphene for optoelectronic [1] and electronic [2] applications. It crystallizes in a layered structure consisting of a sheet of Mo atoms sandwiched between two sheets of S atoms in a trigonal prismatic coordination. The strong intralayer covalent bonding results in very high electrical breakdown current densities [3] and a high mechanical strength [4] of MoS_2 membranes [5]. The weak interlayer interaction renders MoS_2 a well-known dry lubricant [6] and even superconductor upon either intercalation with foreign species like organic molecules and alkali-metal atoms [7,8] or electrostatic doping [9]. As the number of layers of MoS_2 is reduced, this material undergoes a band-gap transition from an indirect band-gap bulk semiconductor to a direct band-gap monolayer semiconductor, showing the significant increase in luminescence quantum efficiency [10,11] and outstanding mechanical properties [12]. The direct band-gap is in the visible frequency range and is, therefore, ideal for optical applications. The lack of inversion symmetry in MoS_2 gives rise to a strong coupling of spin and valley degrees of freedom [13,14], which opens opportunities for valley-based electronic and optoelectronic applications [15]. Logic circuits [16] and amplifiers [17] with high gain based on layered MoS_2 hold great promise for next-generation electronic applications.

Changing the lattice by the application of external pressure or strain without inducing impurities is a clean tool to tune physical properties. There have been theoretical reports demonstrating that MoS_2 monolayers and bilayers undergo a semiconductor to semimetal transition [18,19] and even full metallization [20,21] under biaxial strain. The metallic state of bulk MoS_2 has been theoretically predicted with the application of pressure due to band overlap [22–24]. At pressures above 25 GPa, MoS_2 is believed to have a good figure of merit suitable for practical thermoelectric application [22]. Exploring the metallic state of MoS_2 under pressure is a matter of interest in band-gap engineering. Despite great efforts [25–27] following the pioneering work of Bridgman [28], experimental evidence for metallic MoS_2 upon compression is still absent. Meanwhile, x-ray diffraction (XRD) [29] and Raman spectroscopy [30] indicated a structural transition between 20 and 30 GPa. However, the nature of this high-pressure phase is still undetermined. Whether it links the evolution of the crystal structure and electronic structure to possible metallization remains unclear.

In this Letter, the above-mentioned issues are addressed by combining the resistivity, synchrotron XRD, and Raman scattering measurements on bulk MoS_2 under pressure. We have determined that the pressure-induced transformation is isostructural and is related to a lateral shift of adjacent S-Mo-S layers (see, also, Ref. [24]), which changes the stacking between the layers and results in c-lattice parameter collapse. These effects lead to the change of electronic structure, and the material becomes metallic when the phase transition is complete.

MoS_2 powder samples (Alfa Aesar) were chosen for experiments. Diamond anvil cells (DAC) with Re gaskets were used with anvils in 100 μm culet for the XRD measurements and in 300 μm culet for the Raman

spectroscopy experiments, respectively. Neon was loaded together with samples as a pressure transmitting medium in two runs of XRD experiments. Both neon and argon were loaded as pressure media in two runs of Raman experiments. The monochromatic XRD signals were collected at the synchrotron beam line, sector 13 of the Advanced Phonon Source (APS) of the Argonne National Laboratory and Extreme Conditions Beamline P02.2 at DESY (Germany). The sample-to-detector distance and the image plate orientation angles were calibrated using LaB_6 and CeO_2 standards. For the Raman experiments, a back-scattering geometry was adopted for microconfocal measurements with incident laser wavelength of 488 nm. A quasi-four-probe method was used in a DAC with anvils of 500 μm culet to measure the resistivity of the sample with electrical probes made of platinum foil but without any pressure medium. Pressure was gauged by means of ruby fluorescence [31], equation of state of Au [32], and the diamond Raman shift [33] in these experiments.

The crystal structure of MoS_2 belongs to a space group of $P6_3/mmc$ [34], the repeat unit in the c direction contains two layers, and the S atoms in one sheet are directly above the Mo atoms in the next. This stacking mode is referred to as $2H_c$-MoS_2. We have collected structural data up to 81.0 GPa and the XRD patterns are shown in Fig. 1. All the Bragg peaks shift to larger angles, showing the shrinkage of the MoS_2 lattice. Upon compression to 26.5 GPa, there are several changes in the XRD patterns in the number, shape, and intensity of the peaks, and a new characteristic peak appears at around 3°, in close proximity to the peak of the low-pressure phase. With continuous compression to 36.0 GPa, the new peak takes over, while other changes in diffraction patterns complete. The diffraction patterns remain unchanged after that. When refining these data using a Rietveld method with GSAS software [35], we found that both the low-pressure and high-pressure patterns, indeed, can be described by the single $2H_c$ and $2H_a$ phases, respectively (Fig. 1), while the XRD patterns in the pressure range of 26–36 GPa are the superposition of these patterns in one sample. XRD measurements on another MoS_2 sample up to 60 GPa revealed that the two phases coexist between 20 and 40 GPa (see the Supplemental Material [36], Figs. S1 and S2). Upon decompression, we observed that the transition is reversible, but there is a small hysteresis.

The refined lattice parameters and the unit cell volume of two samples of MoS_2 upon both the compression and decompression run as a function of pressure are shown in Fig. 2 together with other experimental data [27,29] for comparison. Our results agree well with these two sets of data except that the $2H_a$ structure was not identified from previous experimental work [29] and could only be suggested theoretically [24]. In the intermediate range, the parameter a becomes stiffer while the parameter c in $2H_a$ phase drops down. After the phase transition completion, the lattice parameters behave regularly. The lattice parameters in the $2H_c$ and $2H_a$ phases are in excellent
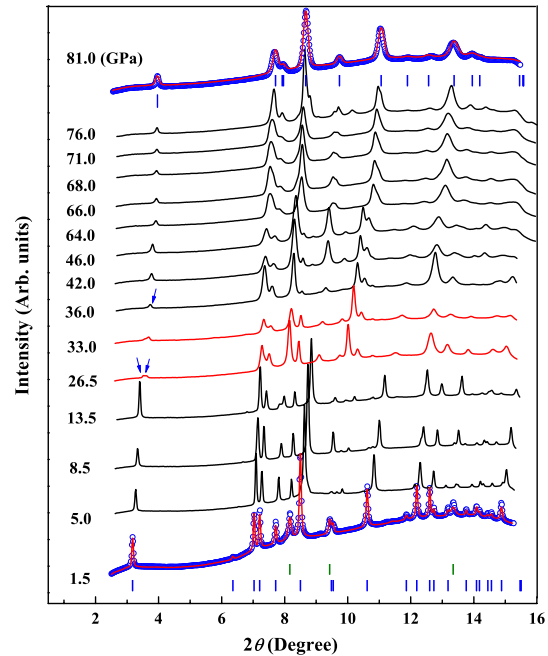

FIG. 1 (color online). Synchrotron x-ray diffraction patterns of MoS_2 during the pressurization from ambient conditions to 81.0 GPa ($\lambda = 0.3344$ Å). Arrows indicate a new peak, which appears at the phase evolution. The observed and Rietveld refined diffraction patterns at 1.5 and 81.0 GPa are shown for the $2H_c$ and $2H_a$ phases. The open circles represent the measured intensities, and the red lines are the results from profile refinements. The patterns shown in red correspond to the mixed phase region. The positions of the Bragg reflections are marked by vertical sticks and the signal from Au in olive sticks. The R values are $R_p = 0.34\%$, weighted profile $R_{wp} = 0.53\%$ at 1.5 GPa and $R_p = 0.69\%$, weighted profile $R_{wp} = 1.15\%$ at 81.0 GPa.

agreement with the theoretical results [24]. The stiff a and reduced c in the $2H_a$ phase suggest a less anisotropic characteristic of the high-pressure phase. The Birch-Murnaghan equation of state [37] provides a good description of the volume-pressure relationship in both phases. Fitting our data points in the $2H_c$ phase, we obtained the ambient-pressure bulk modulus K_0 of 47.65 ± 0.30 GPa with its first pressure derivative $K'_0 = 10.58 \pm 0.08$, and the ambient-pressure volume $V_0 = 106.38 \pm 0.30$ Å^3. Our high-pressure data give $K_0 = 57.86 \pm 0.30$ GPa, $K'_0 = 5.28 \pm 0.01$, and $V_0 = 106.56 \pm 0.06$ Å^3 for $2H_a$. The structural transition from $2H_c$ to $2H_a$ due to MoS_2 layer sliding results in the contraction of the unit cell in about 3.5% at 30 GPa. It is worth mentioning that the obtained K_0 in $2H_c$ is smaller than a value of 53.4 ± 1 GPa with $K'_0 = 9.2 \pm 0.4$ from the data used below 20.5 GPa [29]. Our results were obtained when extending measurements to higher pressure and using a much more effective pressure medium. The hardening bonding feature of $2H_a$ is, thus, reflected by its large K_0 value at higher pressures.

Raman spectroscopy is an effective method for detecting small changes in the lattice, and, to this end, we present a study to support the above conclusions from the XRD data.
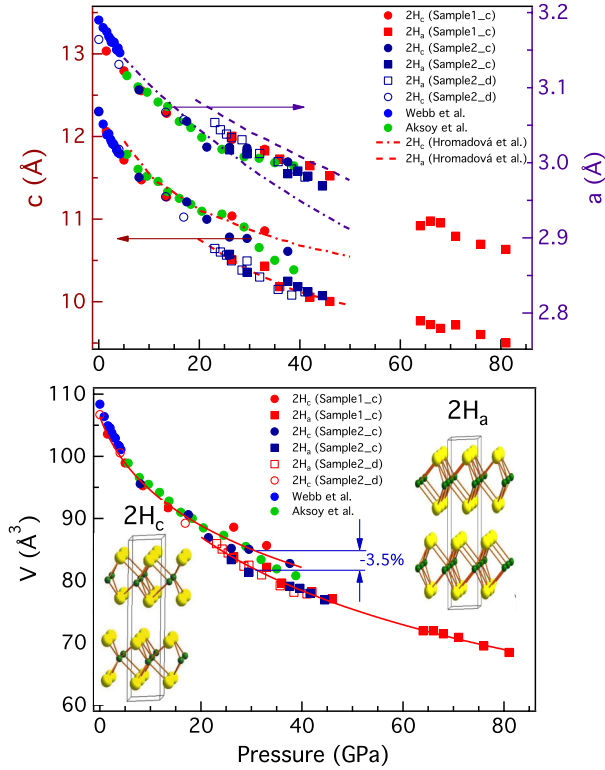
FIG. 2 (color online). Pressure dependence of the lattice parameters (upper panel) and volume per formula unit (lower panel) of two MoS_2 samples in both $2H_c$ and $2H_a$ phases in both the compression (denoted by c) and decompression (by d) run. The experimental data points from Webb *et al.* [27] and Aksoy *et al.* [29], and the theoretical results of Hromadová *et al.* [24] are plotted for comparison. The arrows in the upper panel indicate the corresponding axes. The solid lines demonstrate the fitting data with respect to the equation of states of $2H_c$ and $2H_a$. The insets illustrate the atomic arrangement of the $2H_c$ and $2H_a$ structures where Mo is represented by small spheres and S by large spheres.

Four Raman active modes corresponding to the in-plane E_{2g}^2, E_{1g}, and E_{2g}^1 and the out-of-plane A_{1g} were predicted from a group-theoretic analysis of Γ-point lattice vibrations of $2H$-MoS_2 [38]. The E_{2g}^1 and E_{2g}^2 modes are from the vibrations involved in both Mo and S atoms in the basal plane, with the opposite directions within the MoS_2 unit for the former and the same direction within the unit for the latter. For E_{2g}^2, all three atoms within a MoS_2 unit move in the opposite direction of the neighboring MoS_2. This rigid-layer mode located at the Γ point reflects the weak van der Waals binding force and, therefore, is at a much lower frequency. The A_{1g} mode reflects the vibration of the only S atoms along the c axis, while the E_{1g} mode is from their vibration in the basal plane. We observed all these modes in our high-pressure Raman experiments up to 57 GPa (Fig. 3).

Distinct features were observed through the transition for both the $2H_c$ to $2H_a$ phase where both the E_{2g}^1 and E_{2g}^2 modes develop new split-off features when the applied
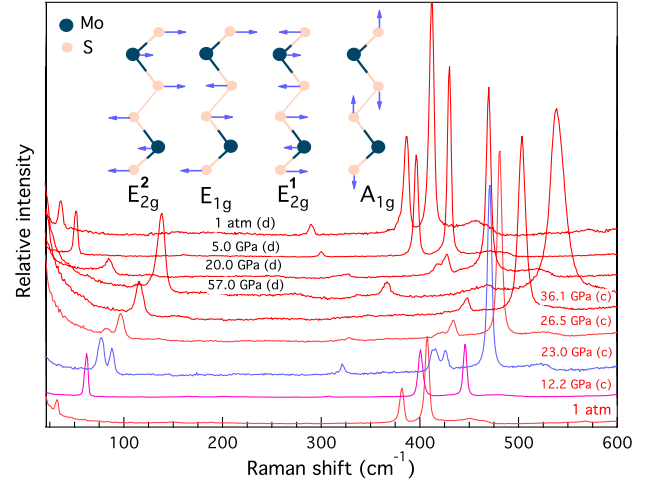

FIG. 3 (color online). Raman spectra of MoS_2 at various pressures up to 57 GPa in both the compression (denoted by c) and decompression (denoted by d) run. The insets represent in-plane phonon modes E_{2g}^2, E_{1g}, and E_{2g}^1 and the out-of-plane phonon mode A_{1g}.

pressure is above 23.0 GPa. The splitting of the E_{2g}^1 was also reported to start at 19.1 GPa in a previous study [30]. This behavior was explained as experimental evidence for the presence of the new $2H_a$ phase due to the layer sliding [24]. We find that the splitting also occurs for the E_{2g}^2 rigid layer mode, which signifies the change in the interlayer stacking mode at the transition. These findings provide consistent evidence with XRD data for the presence of $2H_a$ at high pressures and its coexistence with $2H_c$ in the intermediate range. The two separate peaks for both the E_{2g}^1 and E_{2g}^2 modes of the $2H_c$-MoS_2 phase disappear completely around 40 GPa, indicating that the transformation from $2H_c$ to $2H_a$ is complete, in excellent agreement with the XRD data. Interestingly, we observed the coexisted phases on the pressure release and the recovery to the initial phase at ambient conditions. Thus, both XRD and Raman data provide consistent evidence for the transition, coexistence, and reversibility of the $2H_c$ and $2H_a$ phases.

Figure 4 shows the pressure dependence of the vibrational frequencies and their differences of MoS_2 together with the data from other works [24,30,39]. Consistent with these previous experiments, the E_{2g}^2, A_{1g}, and E_{2g}^1 modes of both $2H_c$ and $2H_a$ phases increase with pressure. We report here the first observation of the high-pressure behavior of the rigid layer mode E_{2g}^2. This mode first increases very rapidly, as it mostly involves weak interlayer van der Waals bonds, and then this rapid increase is gradually slowed down approaching the transition. The rapid increase of this mode resumes in the high-pressure phase. Interestingly, the clear Raman anomalies through the transition are observed for E_{2g}^1 and E_{2g}^2, which involve lateral atomic motion (a slight anomaly for E_{1g} is much more difficult to be observed as this mode is weak), while almost no anomaly is seen for the A_{1g} mode. This is consistent with a radical
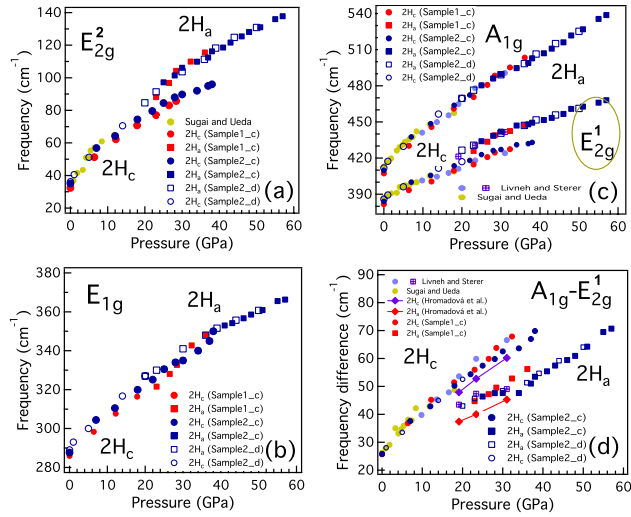
FIG. 4 (color online). Phonon frequencies of MoS$_2$ as a function of pressure with in-plane E_{2g}^2 (a), E_{1g} (b), and E_{2g}^1 modes and the out-of-plane A_{1g} mode (c) and the frequency differences (d) with respect to the corresponding modes. The solid and open symbols are the data for the compression (denoted by $\_c$) and decompression (by $\_d$) run, respectively. The experimental (Refs. [30,39]) and theoretical (Ref. [24]) data points were shown for comparison. $2H_c$ and $2H_a$ are the low-pressure and high-pressure phases, respectively.

FIG. 5 (color online). Electrical resistivity of MoS$_2$ as a function of pressure at room. Insets: Left bottom is the photograph of the sample in the diamond anvil cell with electrical leads at 5 GPa. Upper-right panel shows the temperature dependence of the resistivity of another sample at 28 and 60 GPa.

change in the interlayer stacking and bonding evidenced by structural changes and discontinuities in lattice parameters (Figs. 1 and 2).

Over the pressure range studied, the increase of the E_{2g}^1 vibrational mode is smaller than that of A_{1g}. As a consequence, the frequency difference between these two Raman modes in both $2H_c$ and $2H_a$ is strongly increased with increasing pressure. This difference again clearly evidences the new $2H_a$ phase and the phase coexistence with $2H_c$ in the intermediate pressure range. Note that the obtained trend of the frequency difference with pressure is similar to that for increasing the number of MoS$_2$ layers [40,41].

Next, we present the results for the electronic behavior of this material. Figure 5 summarizes the results of the resistivity as functions of pressure and temperature. The resistivity was found to decrease dramatically with pressure where it levels off to a constant value at around 20 GPa in a compression run. It should be noted that our pressure range is far above the early experiments [25,27,28], which allows for this behavior to be studied further. At 28 GPa, the resistivity-vs-temperature curve shows a semiconducting behavior similar to the ambient-pressure behavior [9,27], exhibiting a strange shape between 100 and 200 K possibly due to the presence of a charge-density wave. However, the temperature-dependent resistivity exhibits a typical metallic behavior at 60 GPa. Pressure-induced gap overlap metallization of the $2H_c$ and $2H_a$ was theoretically predicted between 25 and 35 GPa or at 20 GPa [22–24]. Our results show that MoS$_2$ remains in a semiconducting
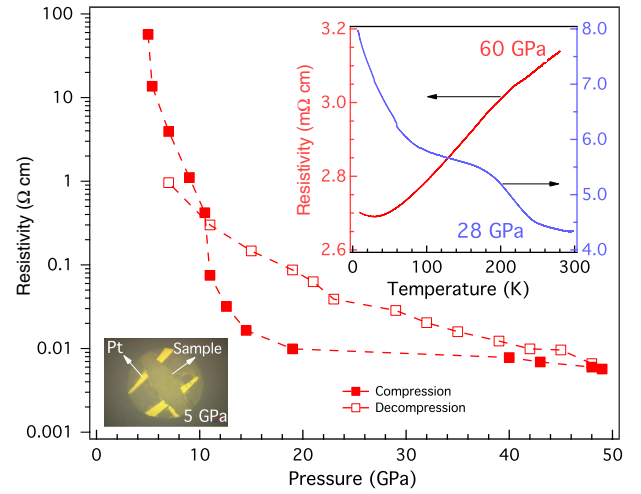
state at 28 GPa, suggesting that the observed metallization takes place in $2H_a$ when the phase transition is complete. It should be noted that the resistivity was found to return to large values upon decompression, which again supports the observed reversibility.

One may be concerned whether the further compression could drive the metallic $2H_a$-MoS$_2$ or other new phase to enter a superconducting state as the case of carrier intercalation [7,8] or injection [9]. Theoretical calculations [24] reveal that $2H_a$-MoS$_2$ has poor metallicity with a dimensionless electron-phonon coupling less than 0.12 at pressures up to 100 GPa, which is not prone to superconductivity. Considering the fact that superconductivity often takes place when some competing order is suppressed by pressure, work is under way to determine the possible superconductivity of MoS$_2$ at higher pressures than reported here.

In summary, we investigated the electrical transport, structural, and vibrational properties of MoS$_2$ by combining the resistivity, synchrotron x-ray diffraction, and Raman scattering measurements. A new $2H_a$ phase was found to occur at high pressures through the first-order phase transformation of the initial $2H_c$ phase, which involves change in interlayer stacking and bonding. A metallic state was achieved in $2H_a$ through lattice contraction when the material undergoes sliding of MoS$_2$ layers and the phase transformation is complete.

Note added.—Recently, we became aware of some similar results in a paper by Nayak *et al.* [42].

———————

*kagayama@stec.es.osaka-u.ac.jp

†xjchen2@gmail.com

[1] Q. H. Wang, K. Kalantar-Zadeh, A. Kis, J. N. Coleman, and M. S. Strano, Nat. Nanotechnol. **7**, 699 (2012).

[2] B. Radisavljevic, A. Radenovic, J. Brivio, V. Giacometti, and A. Kis, Nat. Nanotechnol. **6**, 147 (2011).

[3] D. Lembke and A. Kis, ACS Nano **6**, 10070 (2012).

[4] S. Bertolazzi, J. Brivio, and A. Kis, ACS Nano **5**, 9703 (2011).

[5] J. Brivio, D. T. L. Alexander, and A. Kis, Nano Lett. **11**, 5148 (2011).

[6] W. O. Winer, Wear **10**, 422 (1967).

[7] R. B. Somoano and A. Rembaum, Phys. Rev. Lett. **27**, 402 (1971).

[8] R. B. Somoano, V. Hadek, and A. Rembaum, J. Chem. Phys. **58**, 697 (1973).

[9] J. T. Ye. Y. J. Zhang, R. Akashi, M. S. Bahramy, R. Arita, and Y. Iwasa, Science **338**, 1193 (2012).

[10] A. Splendiani, L. Sun, Y. Zhang, T. Li, J. Kim, C.-Y. Chim, G. Galli, and F. Wang, Nano Lett. **10**, 1271 (2010).

[11] K. F. Mak, C. Lee, J. Hone, J. Shan, and T. F. Heinz, Phys. Rev. Lett. **105**, 136805 (2010).

[12] Q. Peng and S. De, Phys. Chem. Chem. Phys. **15**, 19427 (2013).

[13] K. F. Mak, K. He, J. Shan, and T. F. Heinz, Nat. Nanotechnol. **7**, 494 (2012).

[14] H. Zeng, J. Dai, W. Yao, D. Xiao, and X. Cui, Nat. Nanotechnol. **7**, 490 (2012).

[15] W. Feng, Y. Yao, W. Zhu, J. Zhou, W. Yao, and D. Xiao, Phys. Rev. B **86**, 165108 (2012).

[16] B. Radisavljevic, M. B. Whitwick, and A. Kis, ACS Nano **5**, 9934 (2011).

[17] B. Radisavljevic, M. B. Whitwick, and A. Kis, Appl. Phys. Lett. **101**, 043103 (2012).

[18] W. S. Yun, S. W. Han, S. C. Hong, I. G. Kim, and J. D. Lee, Phys. Rev. B **85**, 033305 (2012).

[19] H. Peelaers and C. G. Van de Walle, Phys. Rev. B **86**, 241401 (2012).

[20] S. Bhattacharyya and A. K. Singh, Phys. Rev. B **86**, 075454 (2012).

[21] E. Scalise, M. Houssa, G. Pourtois, V. Afanas'ev, and A. Stesmans, Nano Res. **5**, 43 (2012).

[22] H. D. Guo, T. Yang, P. Tao, Y. Wang, and Z. D. Zhang, J. Appl. Phys. **113**, 013709 (2013).

[23] C. Espejo, T. Rangel, A. H. Romero, X. Gonze, and G.-M. Rignanese, Phys. Rev. B **87**, 245114 (2013).

[24] L. Hromadová, R. Martoňák, and E. Tosatti, Phys. Rev. B **87**, 144105 (2013).

[25] S. Minomura and H. G. Drickamer, J. Appl. Phys. **34**, 3043 (1963).

[26] G. A. N. Connell, J. A. Wilson, and A. D. Yoffe, J. Phys. Chem. Solids **30**, 287 (1969).

[27] A. W. Webb, J. L. Feldman, E. F. Skelton, L. C. Towle, C. Y. Liu, and I. L. Spain, J. Phys. Chem. Solids **37**, 329 (1976).

[28] P. W. Bridgman, Proc. Am. Acad. Arts Sci. **81**, 165 (1952).

[29] R. Aksoy, Y. Z. Ma, E. Selvi, M. C. Chyu, A. Ertas, and A. White, J. Phys. Chem. Solids **67**, 1914 (2006).

[30] T. Livneh and E. Sterer, Phys. Rev. B **81**, 195209 (2010).

[31] H. K. Mao, J. Xu, and P. M. Bell, J. Geophys. Res. **91**, 4673 (1986).

[32] P. I. Dorogokupets and A. Dewaele, High Press. Res. **27**, 431 (2007).

[33] Y. Akahama and H. Kawamura, J. Appl. Phys. **100**, 043516 (2006).

[34] H. Katzke, P. Tolédano, and W. Depmeier, Phys. Rev. B **69**, 134111 (2004).

[35] A. C. Larson and R. B. Von Dreele, Los Alamos National Laboratory Report No. LAUR 86-748, 1994.

[36] See Supplemental Material at http://link.aps.org/supplemental/10.1103/PhysRevLett.113.036802 for the structural evolution of another sample.

[37] F. Birch, Phys. Rev. **71**, 809 (1947).

[38] T. J. Wieting and J. L. Verble, Phys. Rev. B **3**, 4286 (1971).

[39] S. Sugai and T. Ueda, Phys. Rev. B **26**, 6554 (1982).

[40] C. Lee, H. Yan, L. E. Brus, T. F. Heinz, J. Hone, and S. Ryu, ACS Nano **4**, 2695 (2010).

[41] A. Molina-Sánchez and L. Wirtz, Phys. Rev. B **84**, 155413 (2011).

[42] A. P. Nayak, S. Bhattacharyya, J. Zhu, J. Liu, X. Wu, T. Pandey, C. Jin, A. K. Singh, D. Akinwande, and J.-F. Lin, Nat. Commun. **5**, 3731 (2014).